

Modeling Quench Propagation in Superconducting Cavity Using COMSOL

I. Terechkine

I. Introduction

This note describes an approach to studying quench propagation in walls of superconducting cavities by employing modeling in the COMSOL Multiphysics environment. The main goal of the study was an attempt to evaluate size of a “warm hole” that develops in a wall of a quenching cavity. This hole allows magnetic field generated by magnetic focusing elements placed in the vicinity of a superconducting cavity and activated after the cavity becomes superconducting to penetrate inside the cavity, which results in the drop of the cavity’s quality factor.

Knowledge of the size of the “warm hole” and corresponding quality factor degradation are needed to set some sensible requirements for a fringe field of magnetic focusing lenses installed in the vicinity of a 325 MHz, spoke-type, superconducting accelerating resonator (SSR) of a proton linac front end under study at FNAL within PXIE experiment. In the absence of a ready-to-test SSR cavity, main parameters of this study were chosen to reflect existing tests made at Fermilab TD’s Superconducting Cavity Test Facility (SCTF) using 1.3-GHz, one-cell, elliptical cavities [1]. As one of spoke-type cavities is ready for testing in a vertical test stand of the SCTF, similar tests will be made, and results will be compared with predictions of the developed model.

The model was set so that it could be easily modified to allow using different material properties and geometry parameters. Without significantly compromising the outcome of the study, it was set as a 2-D, axially symmetric, time-dependent, thermal problem with surface energy deposition. The geometry was a 3-mm thick disc with the radius $r_0 = 75$ mm. Quench was initiated in the center of the disc in a small area near the upper surface ($z = 3$ mm). Fig. 1 shows the geometry with the color-coded temperature distribution at the moment $t = 0$.

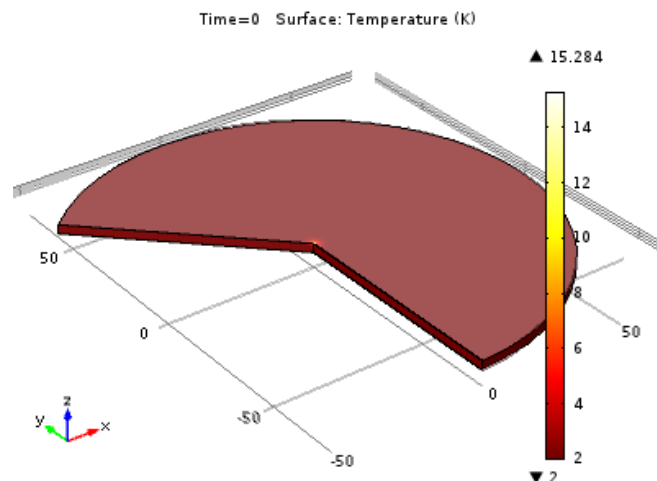


Fig. 1. Study sample with the initial temperature distribution.

It is assumed that we know the energy W stored in the cavity before it quenches; it depends on the level of the surface magnetic field H_t or accelerating gradient E_{acc} . These two quantities are connected to each other:

$$H_t = \eta \cdot E_{acc},$$

where, for 1.3 GHz elliptical cavity, the coefficient $\eta = 3440$ A/MV [2].

On the surface of a superconducting cavity, the energy deposition rate is proportional to a square of the surface current density amplitude J_s :

$$P = 1/2 \cdot J_s^2 \cdot R_s.$$

On the other hand, the current density in the walls of the cavity is directly connected to the stored energy:

$$W = K_{cav} \cdot H_t^2 \equiv K_{cav} \cdot J_s^2,$$

where the coefficient K_{cav} can be readily found for any cavity and any part of its surface [2]; for equatorial zone of a one-cell, 1.3 GHz elliptical cavity, $K_{cav} = 1.3 \cdot 10^{-9}$ J/(A/m)². This expression connects the surface current density in the equatorial area of an elliptical cavity with the energy stored in the cavity. As a result, the next equation for the time derivative of the stored energy can be written:

$$dW/dt = -1/K_{cav} \cdot \int W \cdot R_s \cdot dS$$

The initial value for the stored energy depends on the level of accelerating electric field at the moment of quench, which is usually expressed as an average accelerating gradient E_{acc} :

$$W0 = K_{cav} \cdot (\eta \cdot E_{acc})^2.$$

For a typical average gradient at quench ~ 30 MV/m, $W0 \approx 14$ J.

The differential equation for the stored energy W must be solved simultaneously with the partial differential equation for heat propagation in the cavity wall:

$$\rho \cdot C_p(T) \cdot \partial T / \partial t = \text{div}(\kappa(T) \cdot \text{grad}(T)) + 1/2 H_t^2 \cdot R_s(T)$$

This equation system allows us to find a time-dependent solution for temperature distribution in the wall of the quenching cavity.

The final temperature of the sample (Fig. 1) after quench can be readily found in the adiabatic approximation (that is in the absence of any cooling) by using the enthalpy tables in [3]. With the stored energy $W0 = 14$ J, disc radius $r0 = 75$ mm and thickness $z0 = 3$ mm, the final temperature of the sample after full thermalization $T_{fin} = 16$ K. The immediate conclusion from this observation is that it is enough energy stored in the cavity before quench to bring the temperature of its walls above the transition temperature of Niobium $T_{tr} = 9.2$ K. So, if we need to find the size of the “warm hole” after quench, we must take into account the process of cooling the cavity surface by liquid Helium by employing an appropriate model for this (complicated) process.

II. Material Properties and Cooling by LHe

Heat propagation rate is defined by a diffusion coefficient, which is proportional to a ratio of thermal conductivity K_T to volumetric specific heat C_V . In the expected temperature range, this diffusion factor for Nb can change several orders of magnitude because in the cryogenic environment, both specific heat and thermal conductivity are highly nonlinear functions of

temperature; corresponding graph is shown in Fig. 2. According to this graph, we can expect fast propagation of the normal conducting zone when the temperatures is ~ 10 K, and much slower heat propagation in parts of the sample heated above ~ 20 K. So, we should expect the heat propagation in this case to be highly non-linear, a shock-wave-type phenomenon.

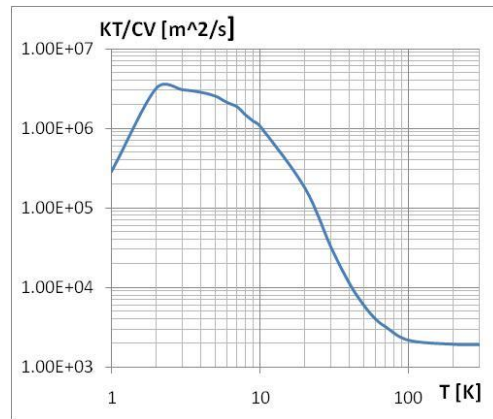


Fig. 2. Heat diffusion factor for Nb in the expected temperature range

Both in the superconducting and in the normal conducting state, relevant material properties, namely specific heat, thermal conductivity, and surface resistance R_s , depend on the temperature in a strongly nonlinear fashion. Besides, these properties depend on the purity of the material and its handling and treatment history. This is one of the reasons of a big spread in known data that characterize Nb at low temperature. While setting the problem in COMSOL, we will assume properties shown in Fig. 3: corresponding data were found in the references [3] to [5].

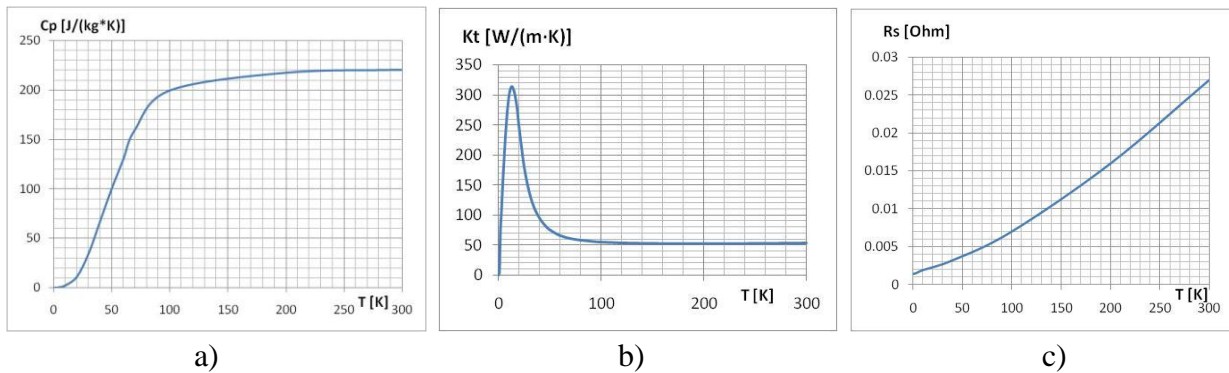


Fig. 3. Specific heat (a), thermal conductivity (b), and surface resistance at 1.3 GHz (c) for RRR300 Niobium.

In the temperature range from 2 K to 300 K, specific heat changes from 0.18 J/(kg·K) up to 220 J/(kg·K), that is about three orders of magnitude. Thermal conductivity of RRR300 Nb changes from ~ 50 W/(m·K) at 2 K to 315 W/(m·K) at 13 K, and then back to ~ 55 W/(m·K) at $T > 100$ K. Surface resistance of normal conducting Nb at 1.3 GHz changes from ~ 1.8 m Ω at 9.2 K to ~ 27 m Ω at 300 K. In the superconducting state, at 1.3 GHz, the surface resistance of RRR300 Nb changes from ~ 2.5 n Ω at 1.8 K to ~ 5.2 $\mu\Omega$ at 9.2 K. Nevertheless, with this, more than three

orders of the magnitude, difference, surface resistance in the superconducting state is more than two orders of magnitude smaller than it is in the normal-conducting state.

To simplify the model, the material properties were parameterized using the next expressions (that can be changed if better approximations are found):

1. **KTT** – thermal conductivity as function of temperature in $W/(m \cdot K)$ is defined as:

32	for $T \leq 1$ K
$32 \cdot T$	for $1 \text{ K} < T \leq 9.5$ K
304	for $9.5 \text{ K} < T \leq 18$ K
$53 + 258420/T^{2.4}$	for $T > 18$ K
2. **CPT** – specific heat as function of temperature in $J/(kg \cdot K)$:
 $220 \cdot (1 - \exp(-1.5 \cdot (T/80)^2))$
3. **RST** - surface resistance in Ω

$(0.001 + 0.00008 \cdot T)$	for $T > 9.2$ K
0	for $T < 9.2$ K

A smoothed step function centered at 9.2 K is used to provide a smooth transition from the normal conducting Nb to the “zero” resistance for the superconducting state. The size of the transition zone of 2 K was chosen; it can be changed though if found too wide.

The start of the quenching process is initiated by assuming the temperature of certain volume of the sample being higher than the transition temperature T_r . This is done by using the next expression for the initial temperature of the sample:

$$T_{|t=0} = T_0 + (T_{\text{init}} - T_0) \cdot \exp(-r/R_0) \cdot \exp(-(z_0 - z)/z_0)$$

The next values of parameters were used: $R_0 = 1$ mm, $Z_0 = 0.3$ mm, $T_0 = 2$ K, $T_{\text{init}} = 15$ K.

Cooling is introduced by choosing an expression for the heat transfer coefficient that is an agreement with data available from reliable sources. For **He-I** boiling at 1 bar, data in [6] were used to derive the next expression for the heat transfer coefficient:

$$k(T) = 80 \cdot (T - 4)^{0.4} + 5000/(T - 4)^2 \quad [W/(m^2 \cdot K)]$$

For **He-II**, the heat transfer data are scarce. Nevertheless, it is possible to use some data available in [7] and [8] to understand that, with the behavior of the heat transfer coefficient as a function of the temperature qualitatively similar to that in the He-I case, higher heat transfer coefficients can be expected. Published data has a big spread; nevertheless, it was possible to derive a simple (but for sure not very accurate) fitting expression for the heat transfer coefficient that works in a wide range of temperature:

$$k(T) = 10 \cdot T + 6000/T \quad [W/(m^2 \cdot K)]$$

Graph in Fig. 4 compares the two expressions for the heat transfer coefficient. Data extracted from the tables in [6] for cooling by liquid helium at 4.2 K are also plotted in this figure for reference.

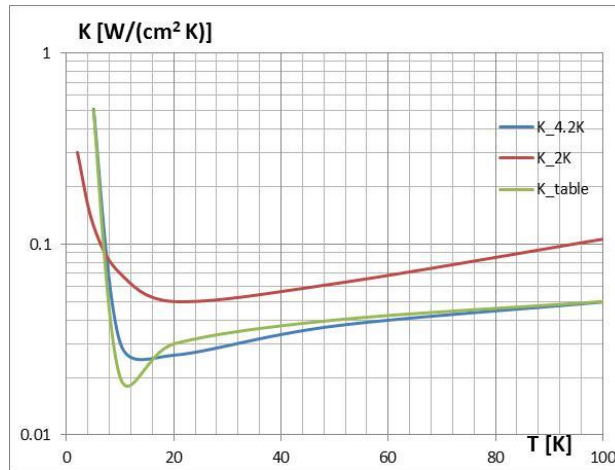


Fig. 4. Heat transfer coefficient into 4.2 K LHe.

As more reliable data becomes available, it can definitely be used to update the model.

III. Results and Discussion

To better understand the quench propagation process, the modeling was made in steps:

- adiabatic approximation with the initial temperature of 4.2 K was used to understand time scale of the heat propagation process;
- 2 K Helium cooling approximation was used to get results in the environment used during cavity tests in [1];
- 4.2 K cooling approximation was used to evaluate the impact of the different implied heat transfer coefficient.

1. **Adiabatic approximation**

Fig. 5 shows evolution of the energy stored in the cavity with **no cooling**. The process of the energy dissipation is over in ~0.5 ms.

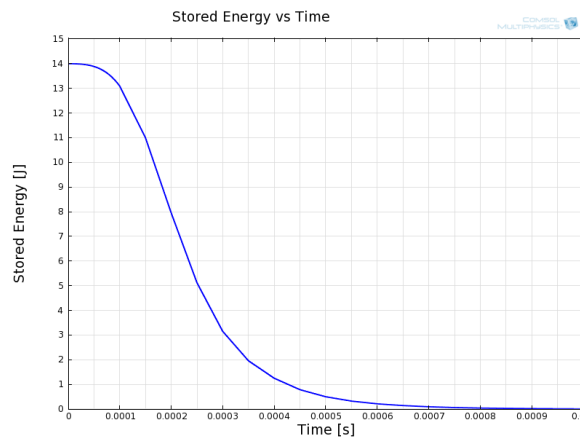


Fig. 5. Stored energy vs time; no cooling

Figures 6 to 13 show temperature distribution along the surfaces of the sample at different moments: as temperature graphs on the left side and as normal conducting (red) zones in the superconducting (blue) sample on the right (pay attention to scales in each figure).

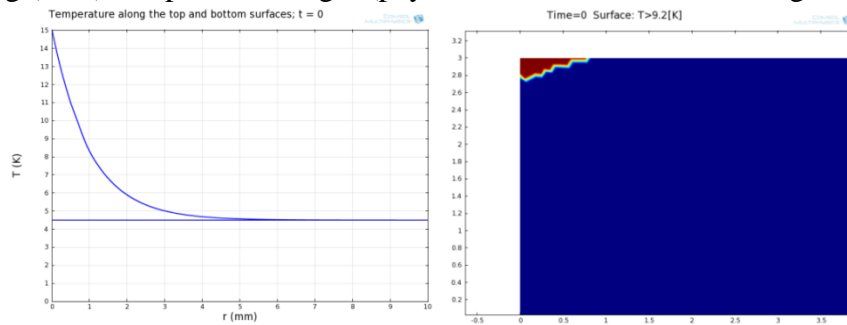


Fig. 6. $t = 0$

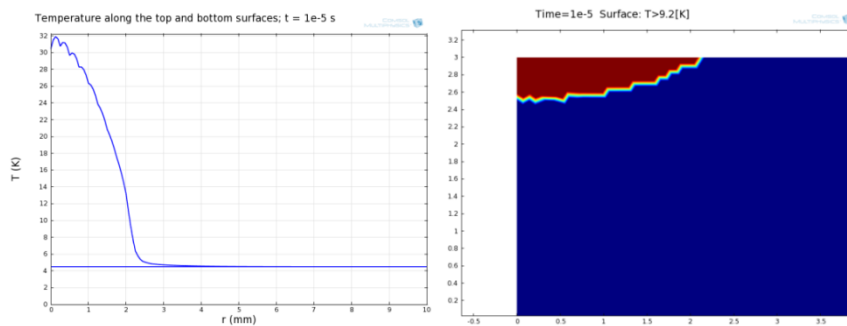


Fig. 7. $t = 1e-5$ s

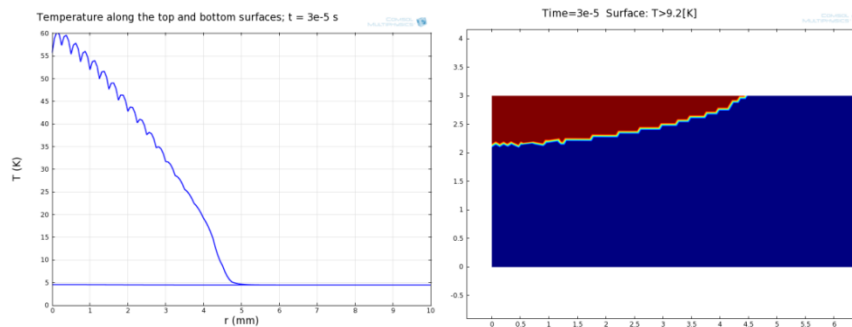


Fig. 8. $t = 3e-5$ s

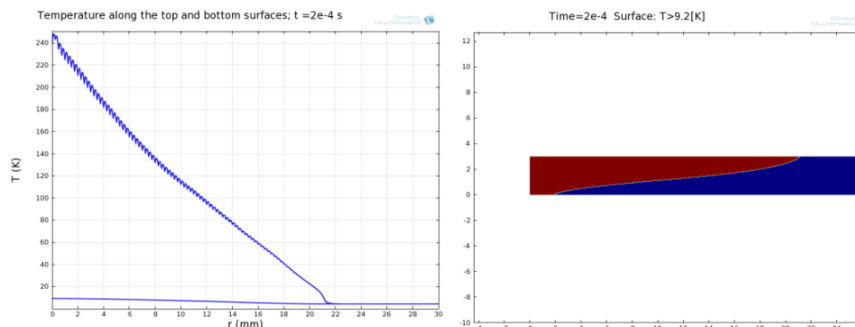


Fig. 9. $t = 2e-4$ s

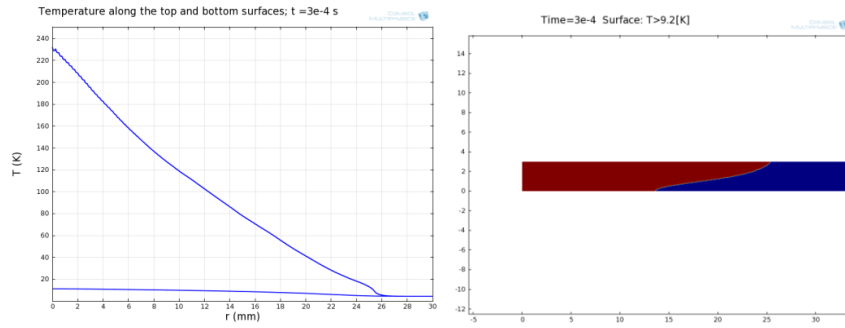


Fig. 10. $t = 3e-4$ s

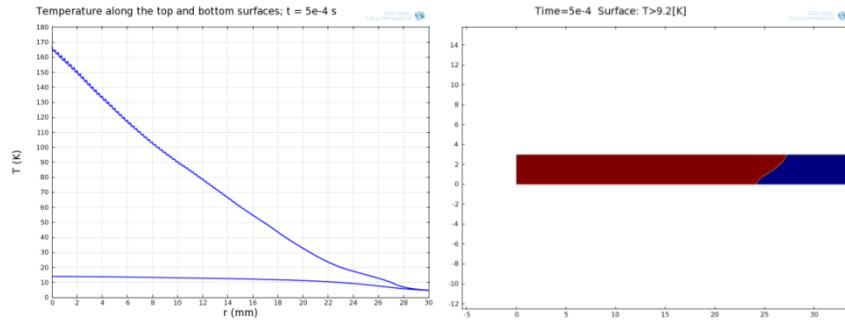


Fig. 11. $t = 5e-4$ s

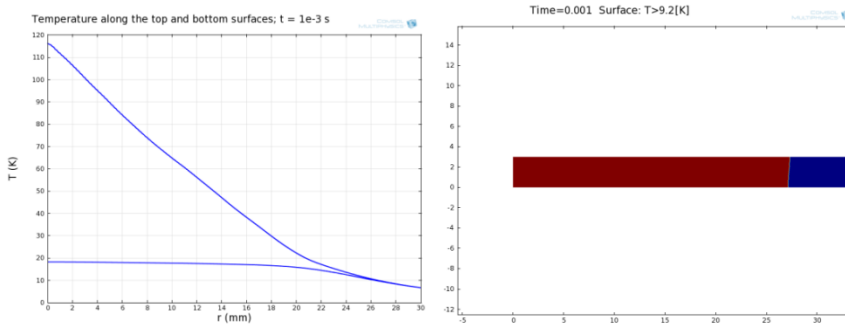


Fig. 12. $t = 1$ ms

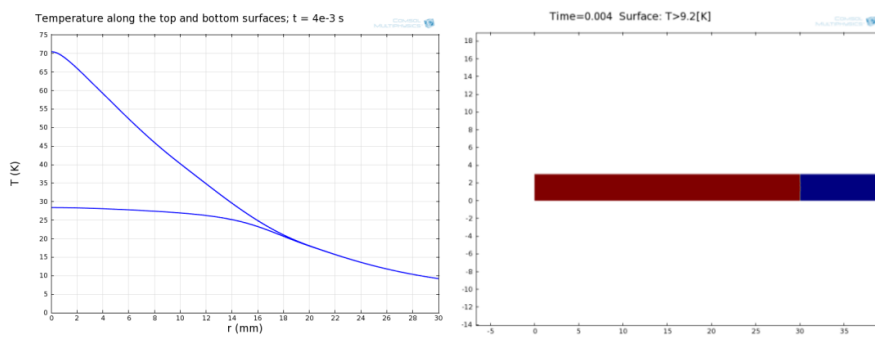


Fig. 13. $t = 4$ ms

Temperature change in time for the top and bottom points on the axis of the sample is shown in Fig. 14.

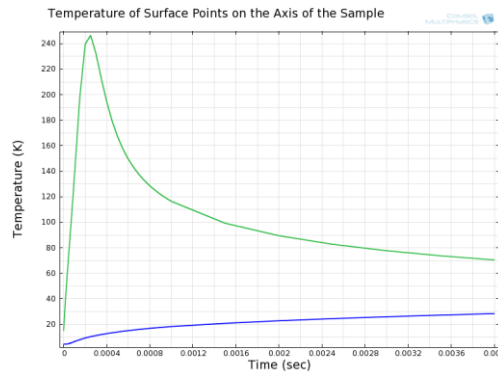


Fig. 14. Temperature change at the top point (green) and the bottom point (blue curve) on the axis of the sample; no cooling

2. Cooling by He-II

The next series of figures show quench propagation when **cooling by He at 2 K** is added to the bottom surface of the sample. We should expect the radius of the warm hole to reach some maximum before the hole starts closing due to cooling. The quench propagation dynamics did not change for the beginning of the process, including the point $t = 4$ ms (Fig. 14), except some (relatively small) difference because of different expressions for the heat transfer coefficients. Figures 15 to 19 illustrate the quenching process. Fig. 15 shows evolution of the stored energy; it should be compared with the graph in Fig. 5 to find that in the case of He-II the dissipation is a bit slower, which is probably a result of different material properties interplay.

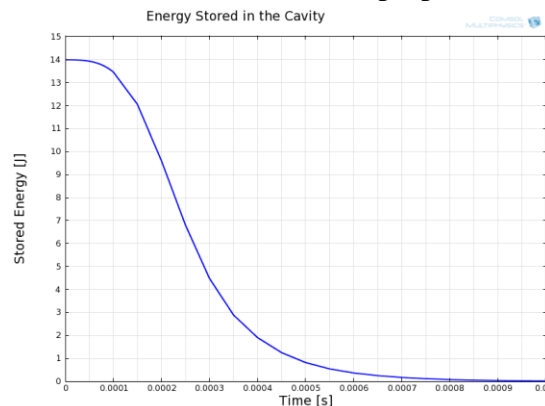


Fig. 15. Energy stored in the cavity as a function of time in the case of cooling by He-II.

Graphs in Fig. 16 show the temperature along the cooled surface at different moments. One can see radial propagation of the quench front during the first millisecond of the process. Gradually, slower processes of heat diffusion and removal by liquid He starts competing with the quench front propagation until the cooling becomes the prevailing process at ~ 50 ms. The sample becomes fully superconducting again at ~ 190 ms.

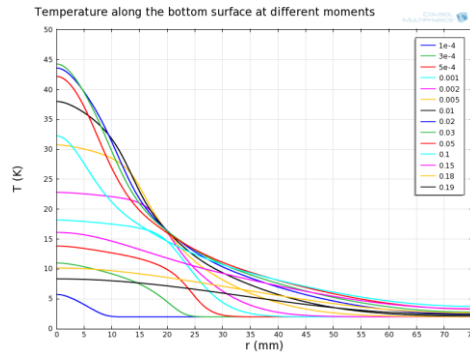


Fig. 16. Temperature distribution along the bottom surface at different moments in time

Comparison of the temperatures at the axial points on the top and the bottom surfaces is made in Fig. 17. The maximum temperature at the heated surface (inside the cavity) is ~ 300 K. It is reached at the very beginning of the process: $t \approx 250 \mu\text{s}$, which is consistent with what was found in the adiabatic approximation. The maximum temperature on the cooled surface (bottom) of ~ 45 K is reached at ~ 30 ms.

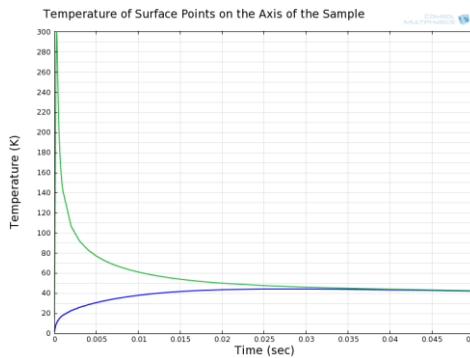


Fig. 17. Temperature of the axial points on the top and bottom surfaces.

In Fig. 18, temperature distribution along the top and the bottom surfaces is shown at the moments corresponding to the maximum diameter of the warm hole (~ 72.6 mm at 70 ms) and complete disappearance of the warm hole (at 190 ms).

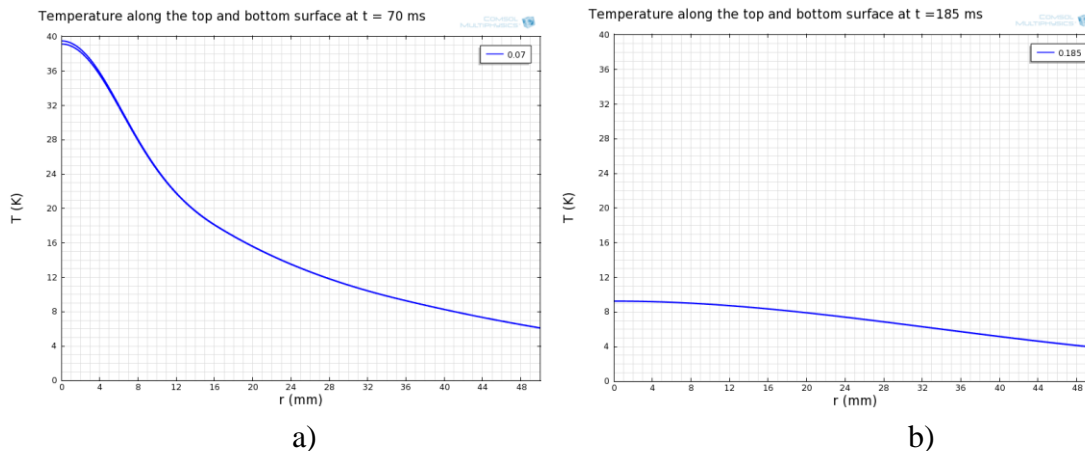


Fig. 18. Temperature distribution along the sample at the moments 70 ms (a) and 190 ms (b).

IV. Conclusion

Although maybe not very precise, results of this attempt to model quench propagation in a superconducting cavity were very useful in providing some visualization of the process and its time scales. This information can be used to compare the data obtained by modeling and by direct measurement of the quality factor degradation of superconducting cavities in the magnetic field of magnetic devices placed in the vicinity of the cavities [9]. With qualitatively very similar behavior of the surface temperature, quantitatively these two methods do not fully converge. Partially the difference can be attributed to a very poor knowledge of the process of cooling by liquid Helium, especially with the temperature difference between the surface and the liquid of ~40 K; this heat exchange issue needs to be better understood. Nevertheless, a “warm hole” size is quite comparable with what was obtained by thermal measurements [10], although precision of the measurements could be better.

Flexibility of how material properties and other variables are introduced in COMSOL makes it straightforward to change the current setting if new or more reliable data sources are found.

Important part of this study is going to be making modeling for higher energies stored in cavities (e.g. nine-cell 1.3 GHz, where the stored energy is of the order of 100 J, or spoke cavities with the energy of ~50 J). With the higher stored energy, non-linear material properties will play even more important role, and computational difficulties increase.

References:

1. D.A. Sergatskov, et al, “External Magnetic Field and Operating SRF Cavity”, SRF-2011, Chicago, 2011.
2. T. Khabiboulline, private communication.
3. “A Compendium of the Properties of Materials at Low Temperature. Part II, Properties of Solids” WADD Technical Report 60-56, NBS, Cryogenic Engineering Division, 1960.
4. “Material Properties for Engineering Analysis of SRF Cavities”, FNAL Engineering Specification 5500.000-ES-371110, Oct 2011.
5. H. Padamsee, J. Knobloch, T. Hays, “RF Superconductivity for Accelerators”.
6. E.G. Brentari, et al, “Boiling Heat Transfer for oxygen, Nitrogen, Hydrogen, and Helium”, US dept-t of Commerce, National Technical Information Service, NBS, Boulder, Colorado, publ. PB-172 323, tech note 317, Sept 1965.
7. H. Padamsee, “Heat Transfer and Models for Breakdown”, 1980 SRF workshop (#1), Karlsruhe, Germany, 1980.
8. S.W. Van Sciver, “He II (superfluid Helium)”, in Handbook of Cryogenic Engineering, ed. J.G. Weisend II, Taylor&Francis, 1998.
9. T. Kabiboulline, J. Ozelis, D. Sergatskov, I. Terechkine, “Superconducting Cavity Quenching in the presence of Magnetic Field”, FNAL note TD-11-020, Dec. 2011.
10. D. Sergatskov, private communication.